Supplementary Information

Probing Antiferromagnetism in Exfoliated Fe_3GeTe_2 Using Magneto-transport Measurements

Stasiu T. Chyczewski[1], Ji Shi[1], Hanwool Lee[1], Paolo F. Furlanetto[2], Kai Xu[1], Arend M. van der Zande[2], and Wenjuan Zhu[1]

[1]Department of Electrical and Computer Engineering, University of Illinois at Urbana-Champaign, Urbana, Illinois 61801, USA
[2]Department of Mechanical Science and Engineering, University of Illinois at Urbana-Champaign, Urbana, Illinois 61801, USA

S1: The transfer process from ref. 1 is adapted for use in this work.[1] All transfer is conducted inside of a nitrogen glovebox in order to minimize the risk of air exposure.

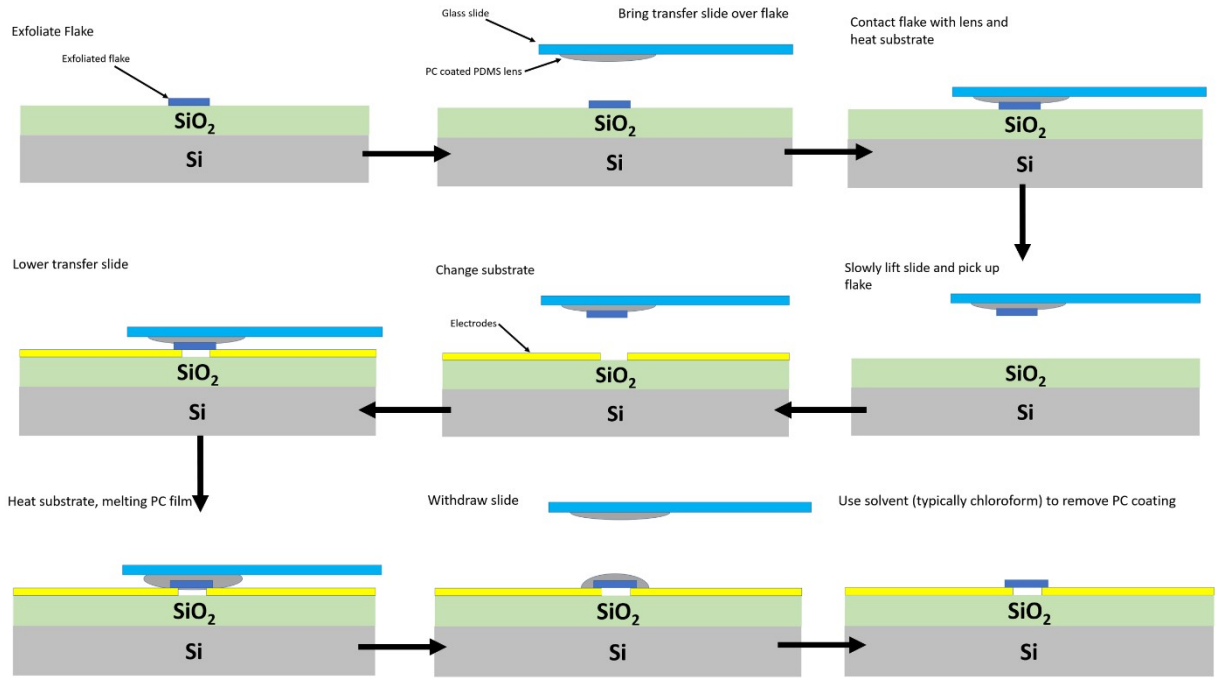

Figure S1: Transfer process used to pick up and place flakes onto an arbitrary target.

S2: Multiple Fe_3GeTe_2 **(**FGT) devices were fabricated in the study. Optical images of several devices (both with and without h-BN) along with corresponding atomic force microscopy (AFM) images are shown below. The FGT flakes in devices 2-6 are about 60 nm, 260 nm, 150 nm, 220 nm, and 30 nm thick. respectively.

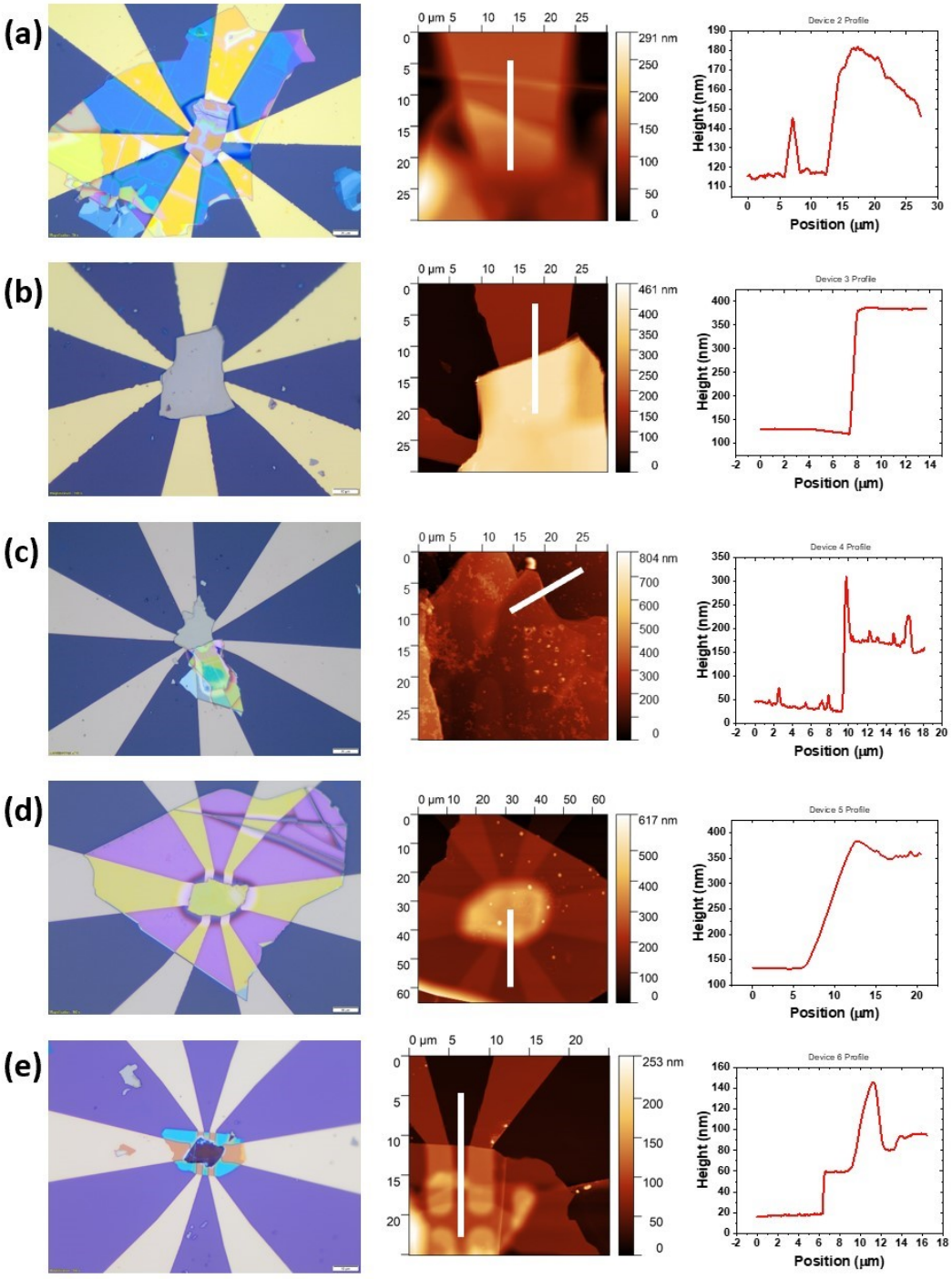

Figure S2:. (a)-(d) Optical images, AFM scans, and extracted height profiles for devices 2-6 respectively.

S3: Electron microscope and EDS mapping of our FGT crystals. By averaging several measurements, we obtained the Fe:Ge:Te atomic ratios of approximately 4.5:1.0:1.8. These results suggest a considerable iron doping in the sample, which explains the observed magnetic switching behavior, including transition temperature, that differs from the commonly reported behavior of Fe_3GeTe_2.

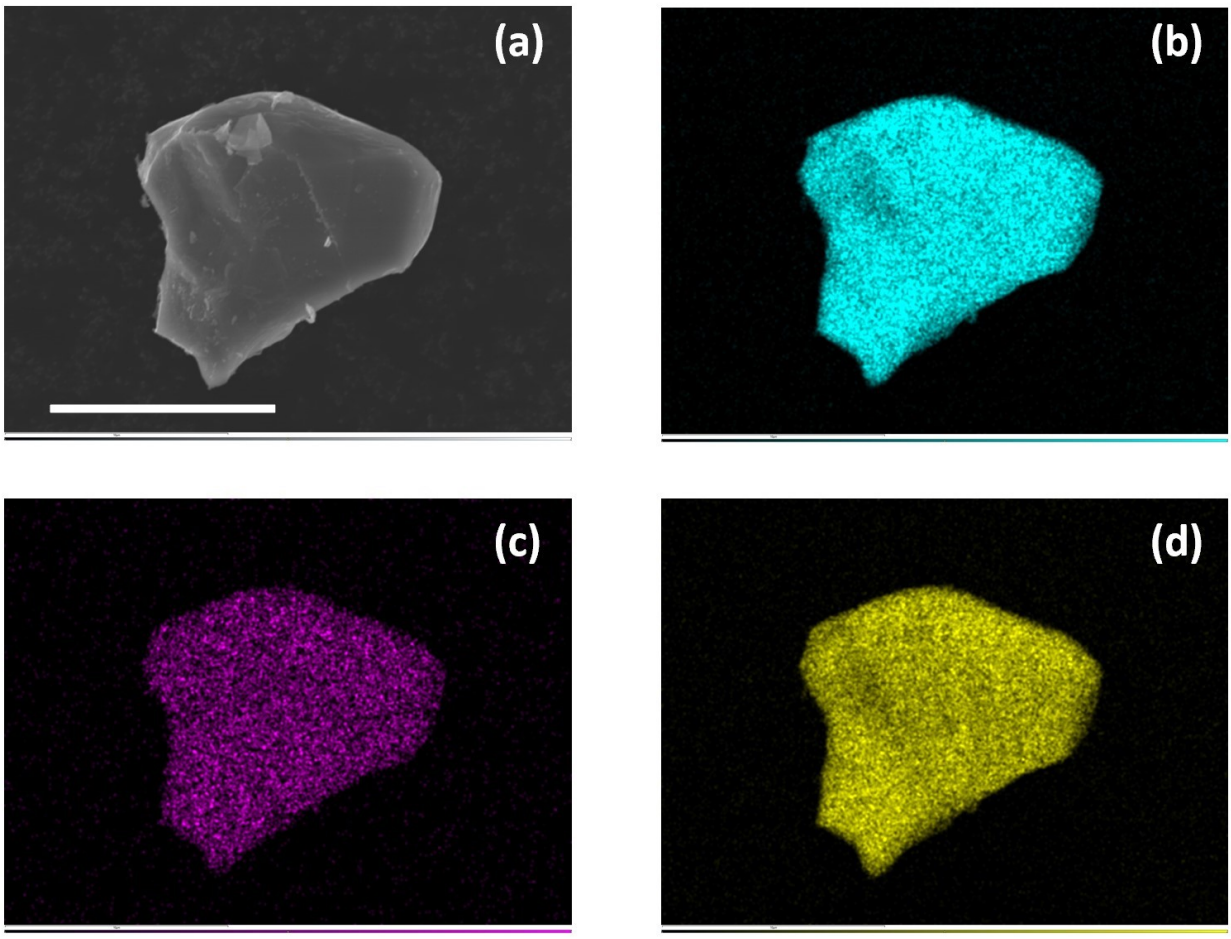

Figure S3: SEM Images & EDS maps of one of our crystals. (a) SEM image of a crystal fragment. (b) EDS scan highlighting iron content. (c) EDS scan highlighting germanium content. (d) EDS scan highlighting tellurium content. Scale bar: 10 μm.

S4: AHE hysteresis loops for 30 nm, 120 nm, and 220 nm devices as well as a comparison of coercivity and remanent R_{xy} for different thicknesses.

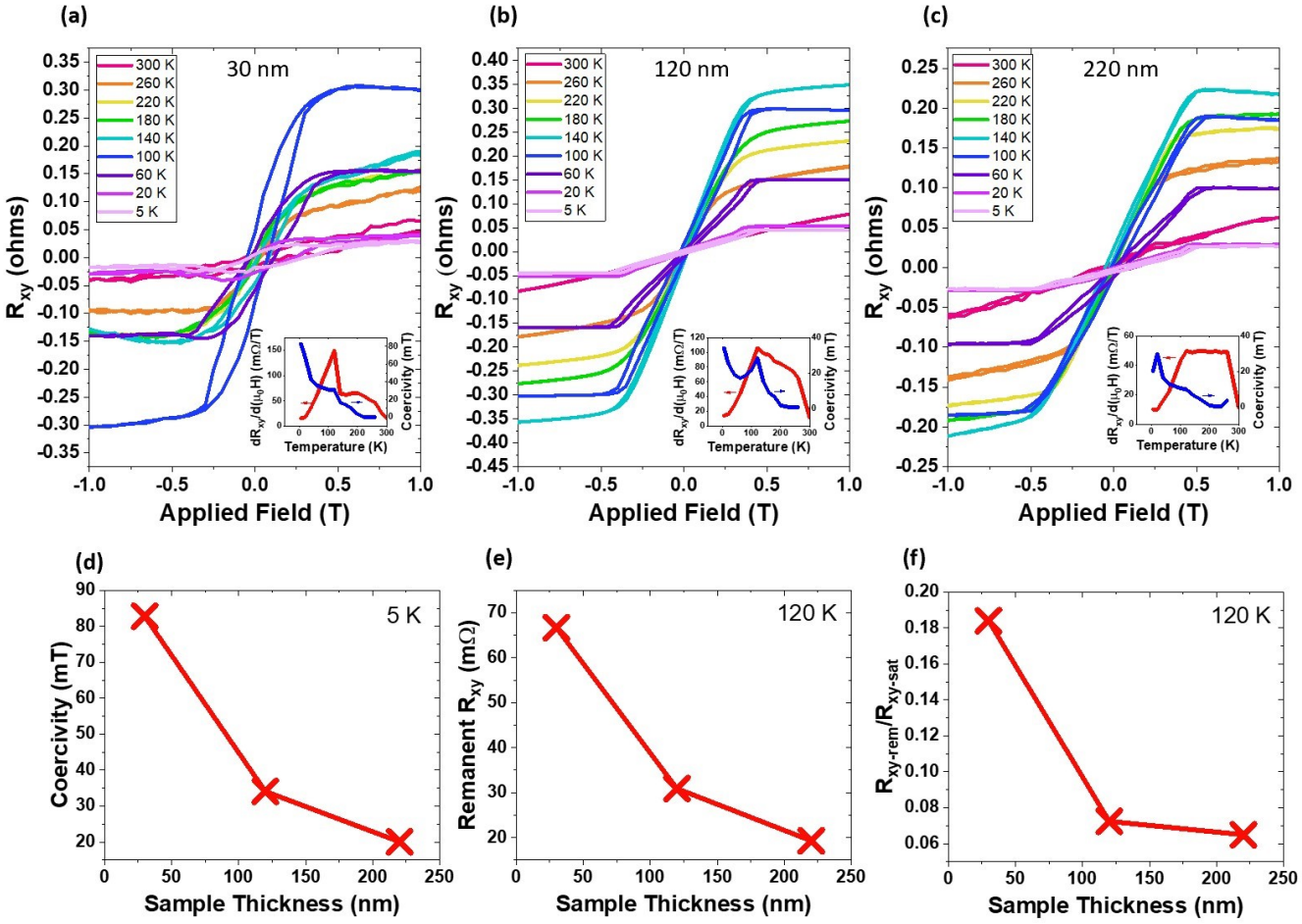

Figure S4: (a, b, c) AHE hysteresis loops for device 6 (30 nm), device 1 (120 nm), and device 5 (220 nm), respectively. Insets show how the derivative of Hall resistance $dR_{xy}/d(\mu_0 H)$ and coercivity changes with temperature. Note that due to contact issues the 30 nm and 220 nm devices have significant contributions from the longitudinal magnetoresistance present in their Hall responses. (d) Coercivity of each device at 5 K. (e) Remanent R_{xy} of each device at 120 K. (f) Ratio of remanent to saturation R_{xy} at 120 K for each device.

S5: Full set of out-of-plane Hall loops for device 1, which features most prominently in the main text. Measurements were conducted at sixteen temperatures from 300 K down to 5 K. Hysteresis loops were first collected at higher temperatures and then at cooler temperatures. The measurement current is 300 μA at 3 Hz.

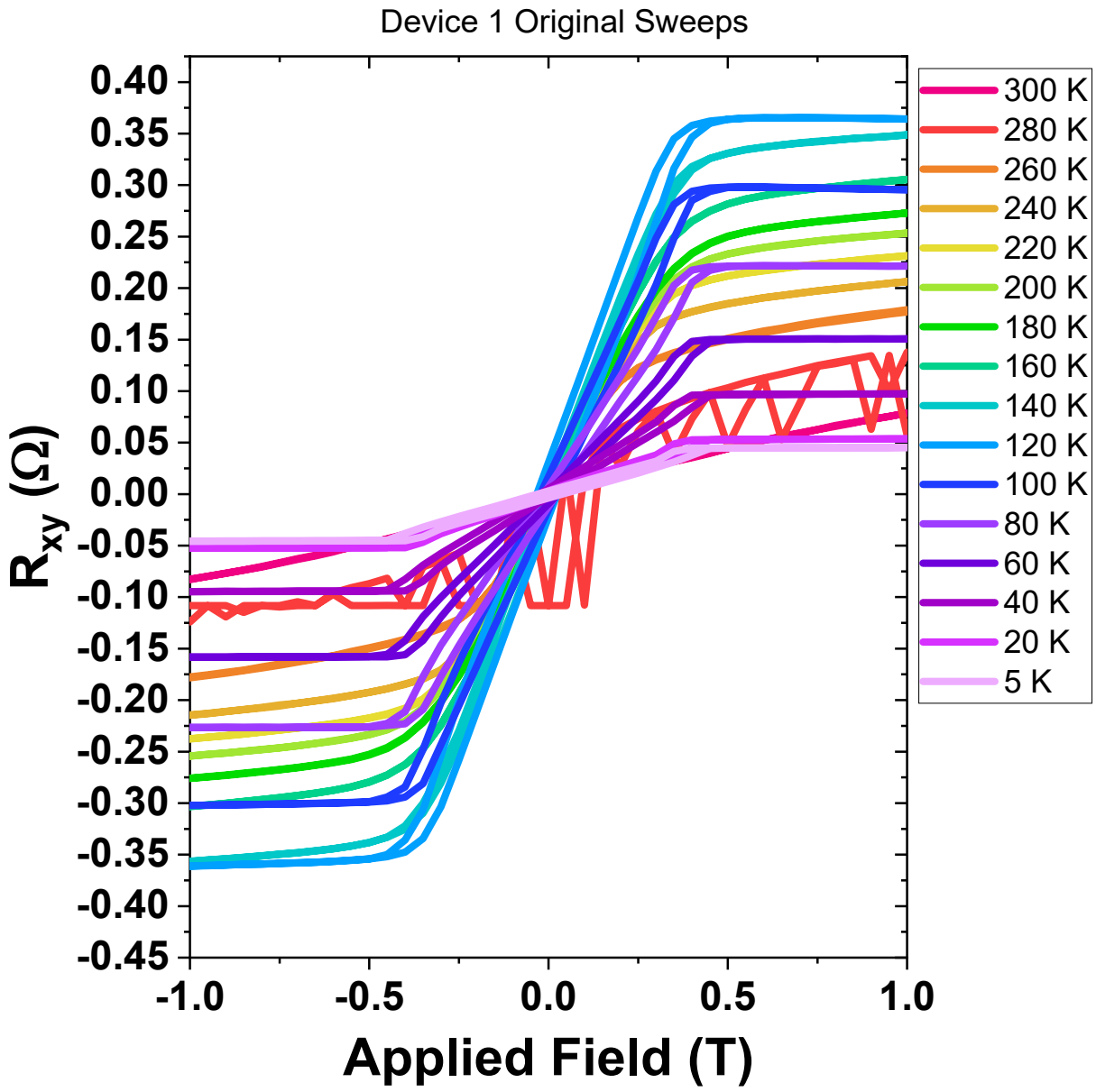

Figure S5: All 16 original Hall resistance sweeps for device 1. Measurement artefacts present in data for 280 K.

S6: anisotropic magnetoresistance (AMR) measurements on device 5 (220 nm thick FGT). The largest magnetoresistance (MR) ratios occur at the measurement temperature of 100 K, consistent with other results. The anisotropic resistance becomes very pronounced as the temperature falls.

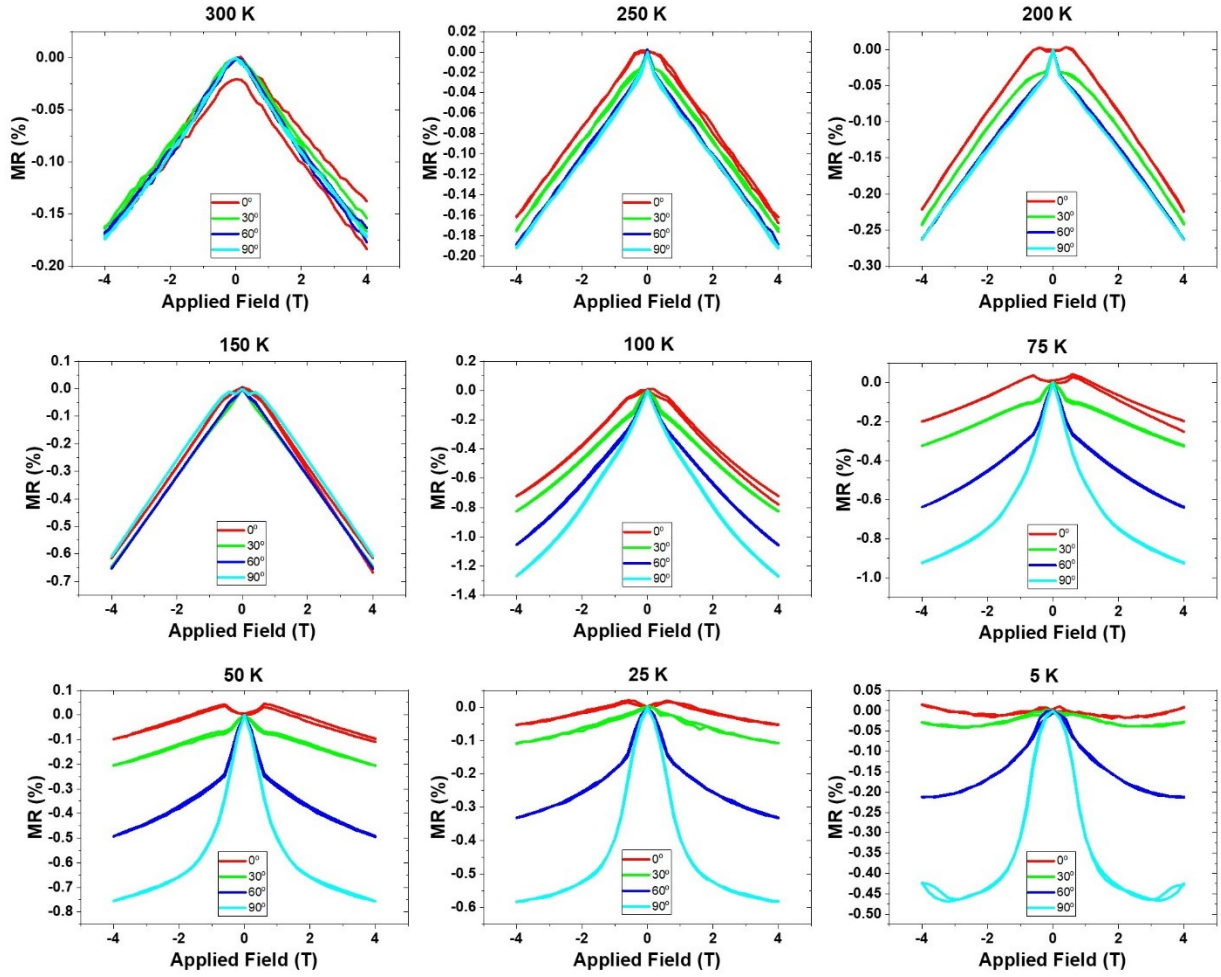

Figure S6: Magnetoresistance measurements in device 5 at various temperatures and angles.

S7: Example anomalous Hall effect (AHE) response of an oxidized FGT flake made with our crystals. This flake is about 42 nm thick as measured by AFM. The steps in the hysteresis loop indicate large areas locally pinned by the antiferromagnetic oxide and have different hysteretic properties as a result.[2] The significant asymmetry in the curve is likely caused by exchange bias.

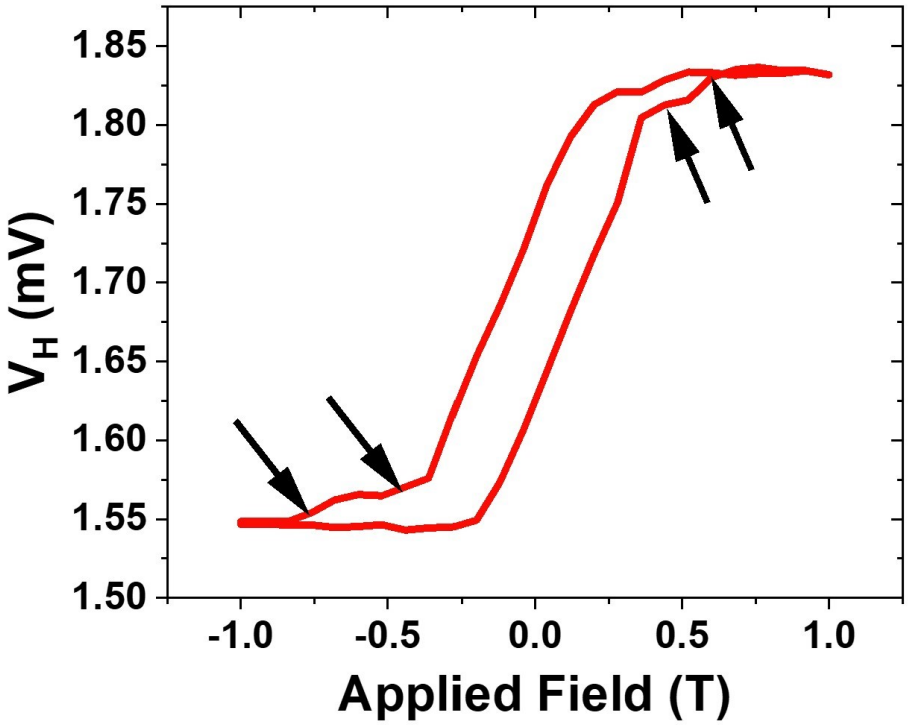

Figure S7: AHE voltage in an oxidized sample. AFM scans on this flake revealed it to be about 40 nm thick. Arrows highlight steps and asymmetries from antiferromagnetic pinning caused by the native oxide.

S8: Additional rotation data for device 1, showing Hall measurements at six different temperatures and four angles at each temperature. Measurement conditions were like those of S5. As mentioned in the main text, the angle dependent behavior changes significantly at lower temperatures.

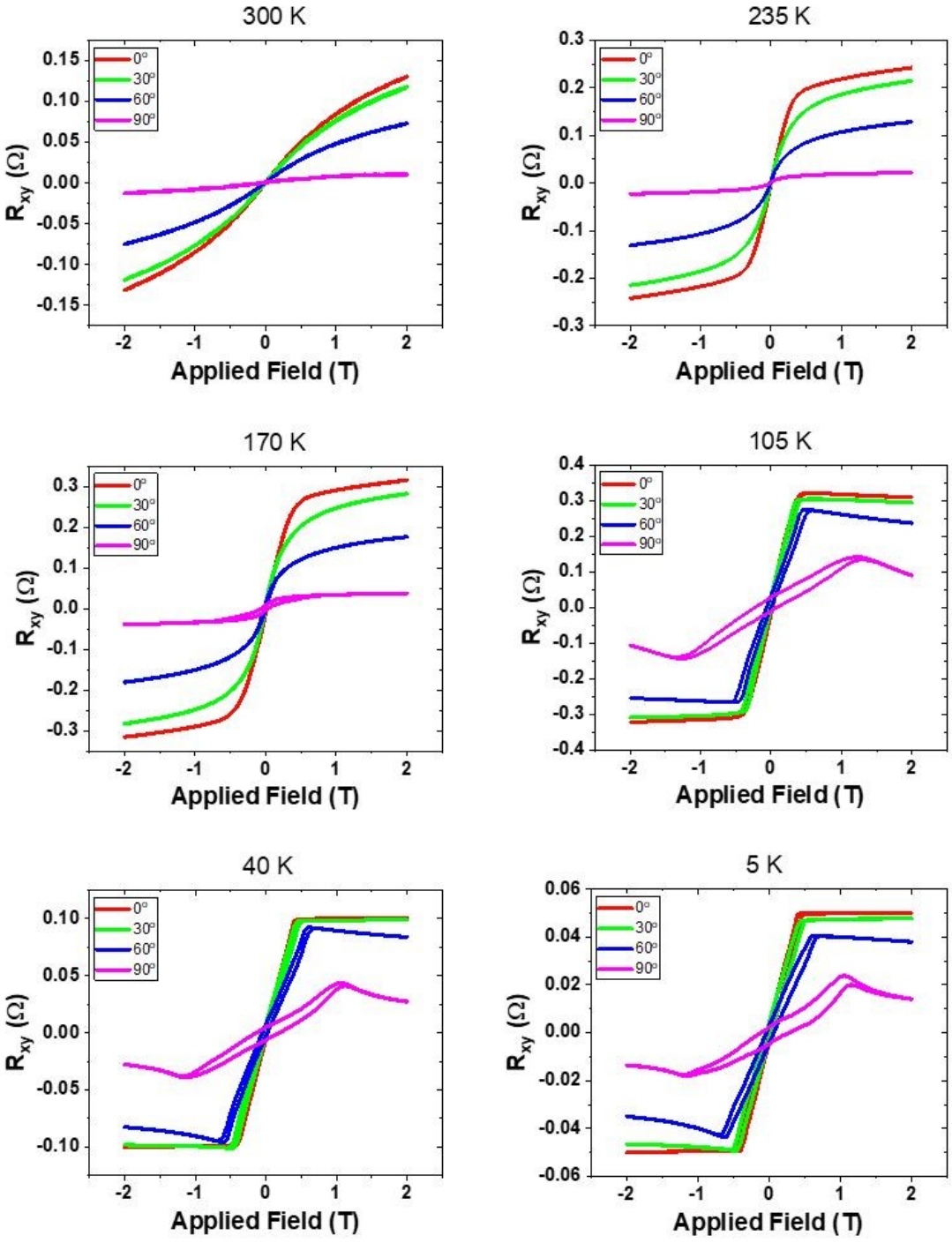

Figure S8: Hall sweeps measured at six temperatures and four angles per temperature for device 1.

S9: Additional field-cooling data for device 1. As mentioned in the main text, the field cooling divergence rapidly vanishes as the sample is warmed.

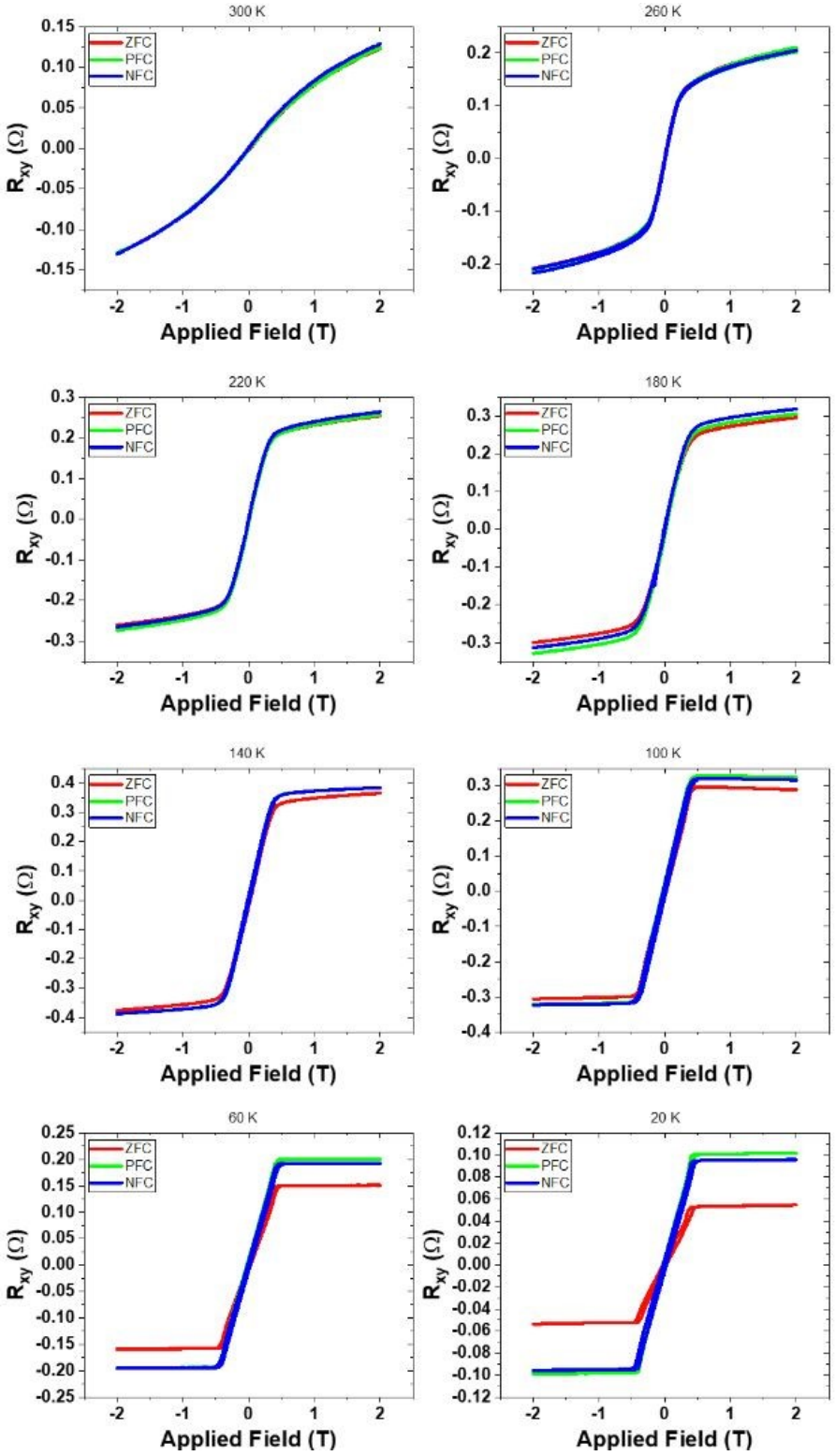

Figure S9: Additional field-cooling Hall sweeps for device 1.

References:

1 Purdie, D. G. *et al.* Cleaning interfaces in layered materials heterostructures. *Nat Commun* **9**, 5387 (2018). https://doi.org:10.1038/s41467-018-07558-3

2 Kim, D. *et al.* Antiferromagnetic coupling of van der Waals ferromagnetic Fe3GeTe2. *Nanotechnology* **30**, 245701 (2019). https://doi.org:10.1088/1361-6528/ab0a37